Design of a Wireless Sensor Node for Overhead High Voltage Transmission Power Lines

Massimo Ferracini, Mario Pagano, *Senior Member, IEEE*, Carlo Petrarca, *Member, IEEE*, Eric Polo, Stefano Saggini, *Member, IEEE*, Giulia Segatti, *Graduate Student Member, IEEE*, and Mario Ursino, *Member, IEEE*

***Abstract*—High Voltage (HV) overhead power lines are systems of interconnected elements that deliver massive amounts of electrical energy over long distances. Electrical conductors, used as energy carriers, are designed according voltage, current, and temperature rated value. Monitoring the power line's state variables is emerging as a crucial topic aiming at both determining the optimal real-time capability and defining a suitable model for Health Index assessment. A Wireless Sensor Network (WSN), consisting of many distributed sensor nodes that communicate with each other, can be a suitable tool to improve line ampacity by maintaining the operating variables in respect of their rated values. This paper investigates the design of an Energy Management System (EMS) for a wireless sensor for HV power line application and proposes a maximum power point tracker (MPPT). The behavior of the MPPT is discussed in terms of electromagnetic field laws and properties of magnetic materials. Ordinary and extraordinary operating conditions are investigated. The theoretical results are validated through a series of experimental tests. A prototype has been realized and tested for real operating currents. The tests are also used to verify the sensor's resilience in the presence of harsh fault conditions.**

***Index Terms*—Overhead power lines, wireless sensor node, energy management system, energy harvesting, resilience, fault condition.**

I. Introduction

SUSTAINABLE energy resources are quickly growing, intending to reduce the non-renewable ones worldwide. For instance, the United States plans to use renewable energy to provide 32% of electricity to the grid by 2030. Many other countries around the world set rules to achieve similar targets. In this context, it is easy to understand how power transmission lines play a crucial role in connecting distributed renewable energy resources to the HV power grids. Overhead transmission power lines are complex systems of interconnected elements and their capability depends on various factors. The first one is, undoubtedly, their technology, so the electrical conductors are designed according to voltage, current, and temperature values. Another factor is the environment in which they are implanted; for instance, two different ampacity values are assigned for winter and summer periods. Also all the solutions implemented to prevent failures are crucial aspects; for example, visual and infrared thermography inspections related to routine programs make it possible to find deficiencies to prevent failures and minimize outages [1]. Intelligent monitoring systems are suitable for improving optimal real-time capability, reducing operating losses, and guaranteeing reliability and safety requirements. Moreover, they allow the automatic detection of faults [2], the design of innovative aging models based on real-time measurements and operational performance evaluation in the presence of external actions. For instance, [3] proposed to equip HV transmission lines with sensors to measure the leakage currents on insulator chains due to pollution and humidity. So, it is evident that today, monitoring power lines' state variables is emerging as a crucial topic to implement new innovative functionalities (i.e., real-time capability, health index assessment and more [4], [5]). In this contest, the candidates to realize the IoT paradigm for HV transmission power lines seems to be Wireless Sensor Networks (WSNs) [6].

They consist of distributed sensor nodes allowing real-time monitoring of physical, mechanical, and environmental conditions (e.g., temperature, mechanical sag, vibration, noise, pollution, etc.). WSNs provide a granular view of the grid and enable new solutions for managing power flow. They allow maximizing the power delivery through the infrastructure, maintaining the power lines inside their safe operating limits. Furthermore, WSNs can be used for sending the collected data to a control room, where data can be observed and analyzed [7].

The design of WSNs for power system application is related to analyzing power requirements, extendibility, and accessibility of the sensors and their power management systems in the presence of relevant electromagnetic fields (e.g., [6], [8], [9]). In particular, a sensor's power requirements for HV power line application are discussed in [8]. The paper highlighted that power consumption is the sum of two terms. The intermittent communication module has an average power consumption of

Manuscript received 24 May 2022; revised 25 September 2022; accepted 6 October 2022. Date of publication 25 October 2022; date of current version 24 March 2023. Paper no. TPWRD-00785-2022. *(Corresponding author: Mario pagano.)*

Massimo Ferracini and Eric Polo are with the Calzavara, 33055 Udine, Friuli Venezia Giulia, Italy (e-mail: massimo.ferracini@calzavara.it; eric.polo@calzavara.it).

Mario Pagano and Carlo Petrarca are with the Department of Electrical Engineering and Information Technologies, University of Napoli Federico II, 80125 Naples, Italy (e-mail: mario.pagano@unina.it; carlo.petrarca@unina.it).

Stefano Saggini and Giulia Segatti are with the Dipartimento Politecnico di Ingegneria e Architettura, University of Udine, 9316 Udine, Friuli-Venezia Giulia, Italy (e-mail: stefano.saggini@uniud.it; segatti.giulia.1@spes.uniud.it).

Mario Ursino is with the PSS, Infineon Technologies AG, 9500 Villach, Austria (e-mail: mario.ursino@infineon.com).

Color versions of one or more figures in this article are available at https://doi.org/10.1109/TPWRD.2022.3216915.

Digital Object Identifier 10.1109/TPWRD.2022.3216915

10^{-6} W, whereas the continuous average power consumption can vary from some hundreds of 10^{-6} W to a few hundred mW. It can be summarized that the actual overall power consumption of a sensor for HV application could be assessed in a few mW. Therefore, the studies on the methods of energizing widely distributed sensors are today a significant challenge.

For instance, [8] and [9] provide an overview of the sensor's energy systems. One possibility is to equip the sensor with an on-board battery. This solution is not very interesting and, at times, not even possible, especially for power lines located in remote localities. The battery needs to be replaced yearly, thus resulting in unfavorable maintenance-free operation [10]. As a result, self-powered wireless sensors (i.e., energy harvesting) are a considerable alternative. This technique allows the sensor to extract energy from the surrounding environment, overcoming the bottleneck of energy-constrained wireless networks.

The energy harvesting systems applied to high voltage transmission line monitoring could be PV panels, wind turbines, thermoelectric, piezoelectric, and electromagnetic field harvesters [11]. Although solar and wind energy technologies represent the most traditional methods for energy scavenging, their utilization for sensors in overhead power lines has many drawbacks, mainly due to high maintenance costs and low reliability of energy source since the extracted power is strongly affected by weather conditions ([12], [13]). Moreover, photovoltaic panels and wind turbines need to be installed on the transmission tower, requiring higher [14] insulation costs compared to direct line-mounted equipment. Furthermore, harsh weather conditions could damage the turbine blades and/or the solar panels. Those systems are considered only in the case of DC lines; for AC lines, the methodologies based on electromagnetic extraction seem to be more promising. Thermoelectric energy harvesters use the Seebeck effect to scavenge energy from the buildup of an electric voltage at the junction between two conductors or semiconductors at different temperatures. Although widespread in many applications [15], to the best of the authors' knowledge, thermal energy harvesting has not been applied in HV transmission systems yet.

Energy harvesting from vibrations is another solution for powering a sensor node [16] and has become prominent thanks to piezoelectric or triboelectric materials. The performances of such techniques are seriously affected by the resonant frequencies of ambient vibrations, which are often random and broadband. Thus, it can be said that vibration energy harvesting is strongly source-dependent. For example, in HV plants, the vibrations of in-service transformers [17] could be used to monitor the equipment [18] as well as to supply power to the sensor nodes. On overhead transmission lines, the sources of vibrations are limited to the wind action or, occasionally, by the operation of circuit breakers. An attempt to implement energy harvesters, using permanent magnets to couple an electromechanical resonator to the current flowing in the nearby HV conductor, can be found in [19]; however, the proposed system is characterized by low power output and decay with the use of the piezoelectric property of lead-zirconate-titanate material.

Due to the constraints of the energy sources, solar, thermal, and mechanical energy harvesting cannot provide a continuous power supply to sensors. Conversely, close to HV overhead transmission lines, electromagnetic energy is abundant due to the intense magnetic and electric fields produced by the electrical currents flowing through conductors operating at high electric potential. Two different energy scavenging techniques can thus be implemented: the first is based on the floating capacitive structure (Electric field Energy Harvesting [EEH]), and the second on the magnetic coupling with the line (Magnetic field Energy Harvesting [MEH]) [20]. The basic idea of EEH relies on using a floating capacitive structure placed in proximity of the high voltage conductor, where a high electric field exists. The harvester gains energy from the displacement current flowing through the parasitic capacitance between the floating electrode and the ground ([21], [22]). Such a technique is widely studied since AC voltage in an operating transmission line is almost stable and not dependent on the conductor's load. The fundamentals of MEH methods are based on extracting the energy from the operating electrical current flowing through the HV conductors: the harvester pulls energy in the manner of a core-clamp current transformer ([23], [24], [25], [26], [27]), as will be shown in detail in the following section. These types of MEH devices need to be clamped around the conductor, and their size and weight are limited to avoid an increase in line sag. Harvesters based on the inductive coupling of a coil and core system placed at a distance from the HV conductor (the so-called free-standing harvesters) have also been proposed: optimized core geometries increase the power output in comparison with a cylindrical magnetic core implementation ([28], [29]). Even if the extracted power depends on the time-varying operating line electrical current, the current transformer method has the great advantage of being typically characterized by higher power densities compared to other energy harvesting solutions ([22], [30]). Thus, it is the most adopted method. In this case, observing that HV power lines also operate in not ordinary conditions (e.g., overcurrents), the current transformer method for WSN has to be also investigated in the presence of these extraordinary currents. Specifically, the transient conditions of the short-circuit currents (when the peaks of the current occur) are the most critical and, hence, have to be the object of analysis.

This paper addresses the design of a wireless sensor's energy management system (EMS) for application on overhead HV power lines. Based on the magnetic coupling approach, the design is carried out by examining, by examining ordinary and extraordinary operating conditions. The proposed new model approach exploits the magnetic material properties to predict the response of the designed system to a broad frequency range input. The method successfully determined the extraction of the maximum power.

In addition, the paper also investigates the resilience of the equipment technology in the presence of harsh failure conditions. In fact, today, Transmission and Distribution System Operators (TSO and DSO) are increasingly interested in concentrating their efforts on ensuring the reliability of electrical infrastructures, making the systems as immune as possible to adverse operating conditions, as in the case of high voltages and currents generated by faults. Indeed, in the present paper, the material response in the presence of short-circuit currents of

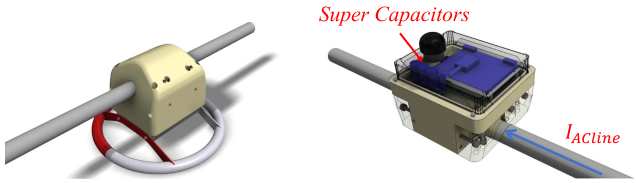

Fig. 1. Sensor node 3D render. (a) sensor with anti-corona device. (b) the bottom view in transparency.

different amplitudes is studied since the possible saturation of the magnetic core could lead to intensified magnetostriction effects and unwanted vibrations; moreover, the generated high-order harmonics could damage the associated electrical circuits.

A section of the paper is focused on the experimental validation of the results of the theoretical analyses. A series of laboratory tests was carried out on a realized sensor prototype. The tests were also performed for high short-circuit current peak values (i.e., the tests were carried out with the values of short-circuit current peaks typically used for Italian HV protection breaker design). It is important to note that during the experimental tests, the measured peak currents (up to 30 kA) were significantly higher than those recorded in similar experimental tests described in the recent literature (i.e., 1700 A in [13]). The success of the tests gave evidence of the resilience of the prototype in the presence of fault conditions. In particular, the tests verified both the resilience of the EMS during the extreme transient conditions and its capability, in terms of power autonomy, to correctly operate during the time following the action of the protection devices (i.e., outage due to line fault or generation trip). The paper is organized as follows: after the Introduction, Section II analyzes the wireless sensor node power management structure; Section III focuses on the magnetic coupling design. Section IV addresses the laboratory arrangement, and Section V discusses the results of the experimental tests; concluding remarks are finally noted in Section VI.

II. Wireless Sensor Node Power Management Scheme

In the proposed application, the sensor monitors online the conductor temperature in an HV transmission line. It detects the temperature and transmits data thanks to a Radio Frequency (RF) module. For its operations, the sensor extracts energy by magnetic coupling from the electrical current I_{ACline} flowing through the HV line conductor. Fig. 1 highlights the 3D rendering of the realized sensor, which is equipped with an anti-corona device. In the figure, the connection of the sensor to the power line is put in evidence.

As already mentioned, one of the most critical aspects of the design of IoT sensors placed inside the nodes of a WSN network is the energy management system (EMS). It controls the sensor power supply operations, simultaneously allowing the two primary operations in low consumption mode: a) disable the parts of the system that are unnecessary; b) recharge the on-board storage device thanks to the energy harvesting operation. Power

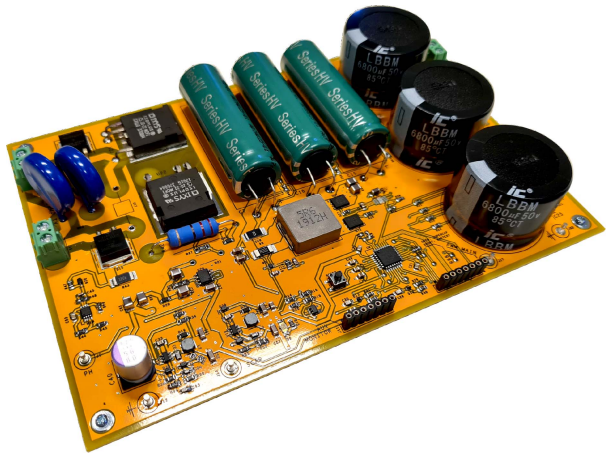

Fig. 2. Energy management board embedded in the case of Fig. 1.

electronic circuits with specific control methods are widely used for voltage conversion and power regulation. Systems typically adopt Maximum Power Point Tracking (MPPT) techniques for impedance matching in order to maximize the power extracted from the source. In [31] an adaptive algorithm is applied to a low-power PIC16F690 microcontroller to adjust the duty cycle of a boost converter to achieve maximum output power. The harvester operates only with line currents ranging from 65 A to 130 A. The device can harvest 58 mW power when placed near a 65 A transmission line. A prototype is developed in [25], which uses the coordination of a compensation capacitor, impedance matching, and short-circuit regulation to maximize output power. It also prevents the magnetic core from saturation. The prototype can deliver 22.5 W power with a 200 A line current. Besides, [32] introduced a desaturation controller, in which the magnetic harvester is composed of two coils. The primary coil harvests energy from the power line, and the secondary coil desaturates the magnetic core. Experimental results show that the proposed device harvests 42.7 mW under a powerline current of 25 A. The circuit increases the amount of harvested power by 5.2 mW through desaturation of the core. Recently, a buck-boost converter operating in discontinuous conduction mode has been adopted in [26] resulting in a peak harvested power of 193.34 mW with a line current of 50 A and a load resistance of 2 kΩ. Although not strictly related to magnetic energy harvesting from HV overhead transmission lines, literature shows a great variety of power electronic topologies and MPPT algorithms; a comprehensive review can be found in [33] and [34].

The EMS studied, realized, and embedded on the board of the sensor prototype is highlighted in Fig. 2. The board is equipped with a supercapacitor-based storage device. Theoretical and experimental tests well know supercapacitor features (e.g., [35]). Their energy density is lower than the electrochemical battery's, but they highlight higher life cycles and broader temperature operating ranges. Monitoring the temperature does not require a high refresh rate, and power peaks are only present when the RF module sends data. In this scenario, supercapacitor

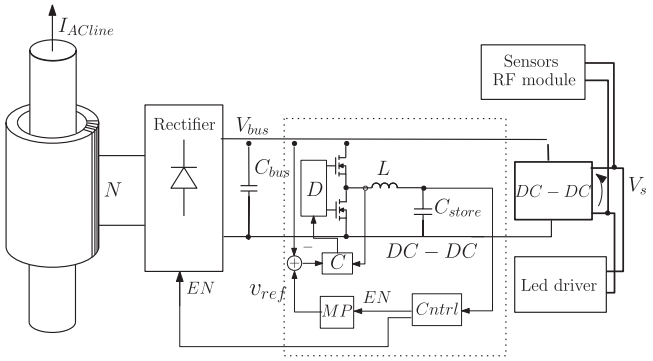

Fig. 3. Sensor node power management architecture.

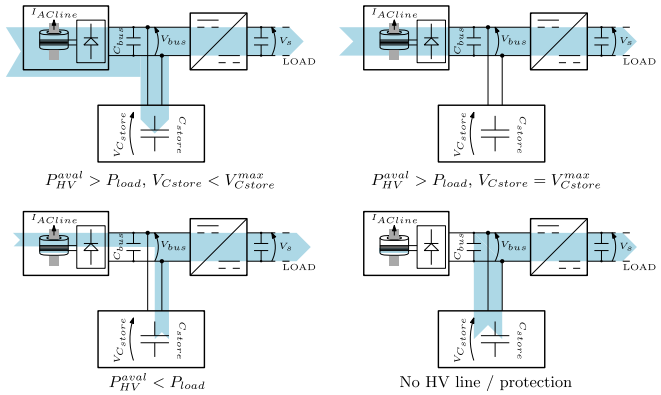

Fig. 4. Power transfer direction during different operating conditions.

TABLE I
POWER MANAGEMENT BOARD SPECIFICATIONS

V_{bus}	12÷60 V
$P_{out,max}$	40 W
f_{sw}	200 kHz
L	SRP1770C-5R6M μH
Size	186×25×126 mm
PCB technology	4 layers, 2 oz
SCRs	CS20-22
Half bridge FETs	SIR170DP-T1-RE3
C_{out}	3×6800 μF
C_{store}	3×HV1860-2R7107-R
MCU	STM32F334K4T6
Control method	Digital peak current control

characteristics, in terms of power and autonomy, suit well to guarantee the sensor's power requirements, and also during the outages of the power line. The leakage current values [36] do not limit supercapacitors' application in WSN (e.g., [37], [38]). Moreover, considering the maintenance cost, in terms of the life cycle, supercapacitors can achieve "perpetual lifetimes" if compared with batteries which, conversely, could require their replacement after a few years [38].

Fig. 3 reports a schematic of the power management architecture developed by the authors. The transformer implements the magnetic coupling system that allows the extraction of a maximum power level that depends solely on the current I_{ACline} flowing along the line. The transformer's output is connected to a controlled rectifier that can be disconnected depending on the control signal *EN*. This solution can be implemented using a bridge with a couple of diodes and SCRs or a diode bridge connected to the V_{bus} by a MOS switch. The voltage level V_{bus} is regulated by the DC-DC power converter connected to the supercapacitor. The main components and characteristics of the power management board are listed in Table I. The actual implementation has been entirely digitally developed with a microcontroller.

Fig. 4 shows the different *power flows* characterizing the system. The operating modes of the energy system depend on the load power requirement, AC current, and supercapacitor voltage. The control block *Cntrl* of Fig. 3 represents the controlling action. If the voltage on the supercapacitor is lower than the maximum value, the *MP* block is enabled. The supercapacitor is charged through a bidirectional buck. The voltage reference of V_{bus} (v_{ref}) is dynamically adjusted to maximize the extracted AC line power through an MPPT algorithm.[1] The loads are disconnected when the supercapacitor voltage is lower than an assigned threshold: this can happen when the AC line carries no sufficient current to keep the system alive. Usually the system will naturally shut down in this condition and resume operation when the AC line has enough current (Fig. 4 does not report this case).

Suppose the total loads (i.e., RF module, sensor, and LED signal lights) require less energy than the available one. In that case, the excess energy is used to charge the storage element, which, in turn, is discharged when the energy supplied by the rectifier is insufficient to power the loads. The rectification is interrupted if the voltage across the supercapacitor is excessively high.

In the case of a short-circuit event affecting the power line, the AC current can rise to tens of kilo amperes: this occurrence cannot be detected before the rectification instant, as no sensor is placed on the conductor; besides, it can also happen when the rectifier is already active. For this reason, an extreme amount of energy can be potentially rectified to V_{bus}. The event can have two effects: the rapid charge of the supercapacitor and, if the rectified current is exceptionally high, the loss of control of the bus voltage. In any case, the system disables the rectification, setting to low-state the *EN* signal level. At the same time, a protection system forces the turn-off instant of the rectifier, and if the V_{bus} voltage exceeds a maximum threshold, a dissipative clamping system activates. It is relevant to note that for the design of a reliable system, in order to correctly assess current and voltage values on the secondary side of the transformer, the accurate modeling of the transformer behavior, even in the presence of short-circuit phenomena, is necessary. This topic will be addressed in the following section.

III. MAGNETIC COUPLING DESIGN

The magnetic coupling is based on a laminated ferromagnetic core of cylindrical shape closed on the line conductor, as shown

[1]The controller calculates the input power through direct current and voltage measurements, and periodically oscillates the reference bus voltage to track maximum power extraction.

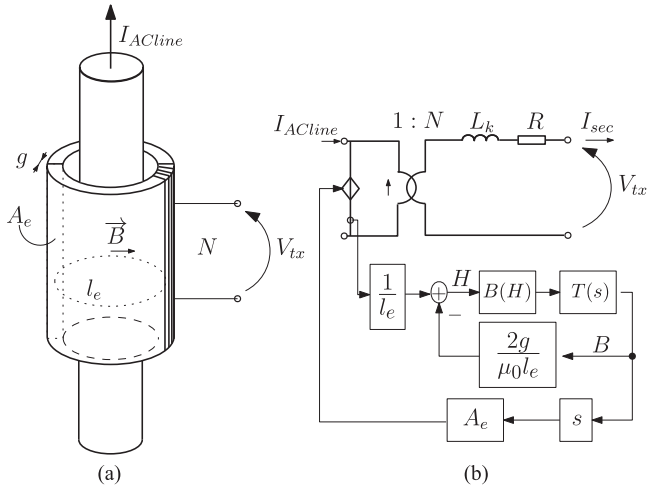

Fig. 5. (a) Transformer shape, (b) Detailed model of the non-linear transformer.

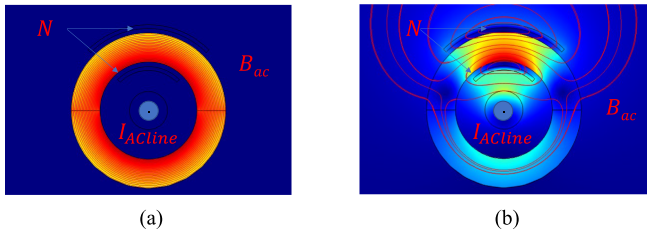

Fig. 6. Magnetic field simulation in the horizontal cross section of Fig. 5 in two cases: (a) magnetizing flux lines present when $I_{ACline} \neq 0$ and $I_{sec} = 0$, (b) leakage flux lines present when $I_{ACline} = -NI_{sec}$.

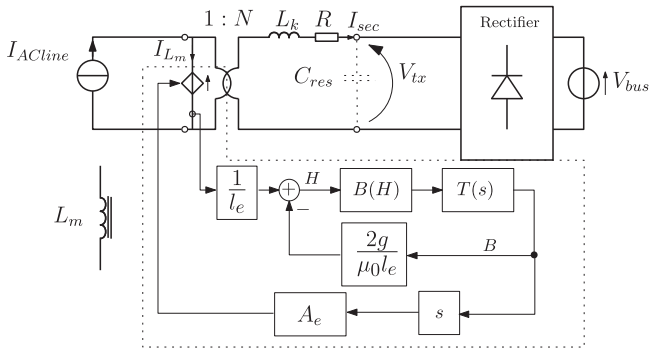

Fig. 7. Equivalent circuit with transformer model considering a regulated V_{bus} voltage.

in Fig. 5(a). On the magnetic core, there is a secondary winding with N turns. For reasons related to mechanical assembly, the magnetic core is realized by joining two halves of laminated steel, resulting in an unwanted air gap called g in Fig. 5(a). The main geometrical parameters of the transformer are the equivalent cross-section area A_e and the equivalent length l_e, equal to the perimeter of the circumference, with an average diameter between the internal and external diameter of the ferromagnetic cylindrical core. The magnetic component's design determines the device's capability in terms of maximum power and short-circuit resilience, that is, the ability of the system to recover from the effects of a short-circuit event on the AC line.

The peculiarity of this project is that system functionality depends on core $B(H)$ non-linear characteristic and the frequency behavior of the magnetic permeability. For this reason, the system must be appropriately modeled, as shown in Fig. 5(b). The $\overrightarrow{H}$ field in the core can be derived by the following relation:

$$\oint \overrightarrow{H} dl \cong H l_{eq} + 2 H_g g = I_{ACline} - I_{sec} N \qquad (1)$$

where I_{sec} is the current in the N turns of the secondary winding. The flux density $\overrightarrow{B}$ is derived from the material's $B(H)$ curves and the transfer function $T(s)$. $T(s)$ is a low-pass filter that models the frequency behavior of the equivalent permeability. $T(s)$ summarizes the behavior of the core in a wide range of frequencies. The analysis is based on a homogenization approach that considers the laminated core as a material described by a complex permeability in a wide range of frequencies. This transfer function plays an essential role in the project because the resilience of the sensor to a short-circuit fault depends solely on this characteristic. L_k considers the leakage flux (reported in Fig. 6(b)), and R is the equivalent secondary winding resistance. The two gaps g generate feedback in the system derived from the relation (1) since $H_g = B/\mu_0$. For each current level, I_{ACline} in the line, the main sizing parameters of the transformer for a given application are derived from the circuit shown in Fig. 7.

The line current is modeled as an ideal current generator I_{ACline}, and the rectifier circuit is connected to the transformer model. The DC-DC converters with the other equipment reported in Fig. 3 are modeled as the voltage source V_{bus}. In fact, the DC-DC converter connected to the super-capacitor controls the bus voltage V_{bus} by regulating the current of the storage element: this is a buck converter with its feedback at the input. Considering the super-capacitor in charging condition, the first harmonic approximation model of circuit Fig. 7 is shown in Fig. 8(a). In this scheme, the transformer is described by the magnetizing inductor L_m and the resistor R_{los} that depend on the voltage drop V_d to take into account the non-linear characteristic of the core. The rectifier is modeled as the impedance Z, whose absorbed power represents the power extracted from the harvesting circuit. This impedance depends on the regulated voltage V_{bus}. This schematic describe the relationships between the main quantities that define the magnetic design. The curve of Fig. 8(b) represents the extracted power P_{ext} as a function of the voltage V_{bus} for the circuit of Fig. 7. The peak power of Fig. 8(b), obtained for V_{bus} equal to V_{MP}, represents the maximum power extracted for a given current line condition. The presence of maximum obtainable power is inherent in the presence of an impedance in parallel to the current generator in the model of Fig. 8. For simplicity, the maximum power extraction will be analyzed without considering the saturation. For V_{bus} up to V_{MP}, V_{tx} is approximately a square wave with amplitude V_{bus}. In this condition, the main circuit waveforms are reported in Fig. 9, in which the line current I_{ACline}, the magnetizing inductor current I_{L_m} and the secondary current I_{sec} are shown.

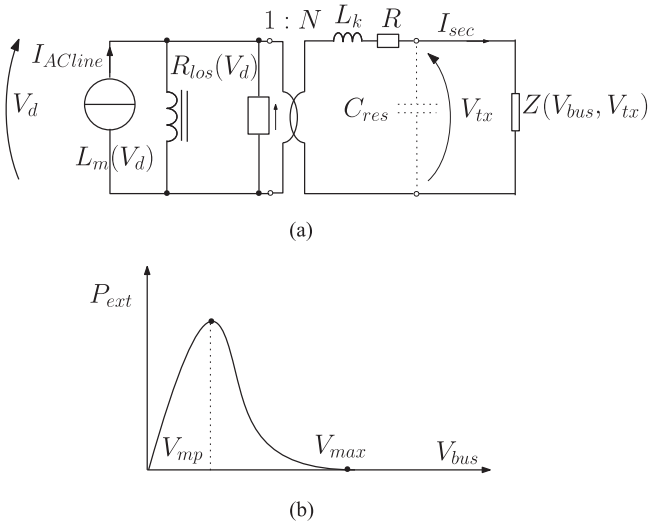

Fig. 8. (a) First harmonic approximation model of circuit of Fig. 7(b) output power P_{ext} as a function of V_{bus}.

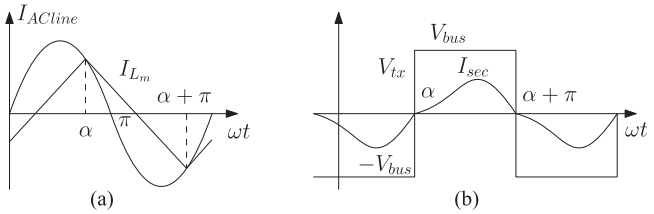

Fig. 9. (a) Waveforms of the line current I_{ACline} and the magnetizing inductor current I_{Lm}, (b) Waveform of the secondary current I_{sec}.

For the sake of simplicity, neglecting the effect of core loss and the leakage inductance L_k, the angle α can be derived as:

$$\alpha = \pi - \phi \tag{2}$$

where

$$\phi = \arcsin\left(\frac{V_{bus}T}{4\,NL_mI_{ACline}}\right) \tag{3}$$

Under these conditions, the total active power transmitted to the secondary will be:

$$P_{ext} = \frac{2V_{bus}I_{ACline}}{\pi N}cos(\phi) \tag{4}$$

where I_{ACline} is considered the peak ac current value. In this case, the maximum of the relation (4) as a function of the voltage V_{bus} approximates V_{MP}. In formula:

$$V_{bus,max} = 2\sqrt{2}\frac{NL_mI_{ACline}}{T} \tag{5}$$

So, the maximum power can be expressed as:

$$P_{ext,max} = \frac{4L_mI_{ACline}^2}{\pi T} \tag{6}$$

For higher voltages, the diodes no longer operate in continuous conduction mode, and the waveforms of Fig. 9 do not represent the circuit operation. The power as a function of the voltage V_{bus} is lower than that predicted by (4) until it is zeroed

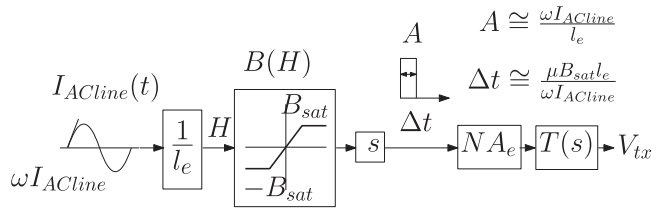

Fig. 10. Diagram with the phases of generation of the maximum voltage in the event of a short-circuit on the AC line.

at the point V_{max}, which represents the peak of the maximum voltage on the magnetizing inductance L_m at the zero crossing of I_{ACline} reflected to the secondary. The maximum power extracted for a bus voltage equal to V_{MP} is maximized by increasing the value of the magnetization inductance, hence, by reducing both the mounting gap g and the equivalent length l_e, and by increasing both the equivalent area A_e and the permeability μ_r. The value of N is chosen so as to adjust the voltage level of V_{MP} at the desired value, which allows to manage the power supply voltage levels in the sensor.

(4)–(6) can be a summary approximation of the maximum extractable power only if the core is not saturated. The core saturation is not present if the following relation is satisfied:

$$V_{bus} < \frac{4B_{sat}A_eN}{T} \tag{7}$$

where B_{sat} is the saturation flux density of the material, A_e is the equivalent area of the core, N is the number of windings, and T is the period of the grid voltage. As long as condition (7) is satisfied, the behavior of the core can be effectively described using a constant magnetization inductance L_m, as reported in Fig. 8. Moreover, as reported in [39], the energy extraction can be further increased by using a resonant capacitor C_{res} connected in parallel at the secondary side of the transformer that increases the total impedance connected in parallel to the current generator I_{ACline}. This solution is effective until there is saturation, which reduces the equivalent value of L_m.

The (3) and (4) are to be considered approximations that allow the description of the quantities that affect the magnetic design and a maximum dimensioning of the system. Considering also a partial intervention of the saturation and the effect of the other parasitic components, the actual extraction of the power must be obtained starting from the circuit of Fig. 7.

Another critical parameter to be considered in case of a short-circuit event is the voltage V_{max}, which represents the open-circuit voltage. This value represents the maximum voltage level present in the circuit of Fig. 7 and is needed for a suitable selection of the rectifier components.

At very high line currents, the core will be fully saturated for almost the entire period T. The most critical moments are the zero crossing of the current, in which the core is not saturated, and in which the time derivative $dI_{ACline}(t)/dt$ is maximum. Under these operating conditions, the transfer function $T(s)$ plays a key role. The simplified scheme of Fig. 10 can be used in order to understand the process that defines the maximum amplitude V_{max} of the voltage pulses in the open circuit condition

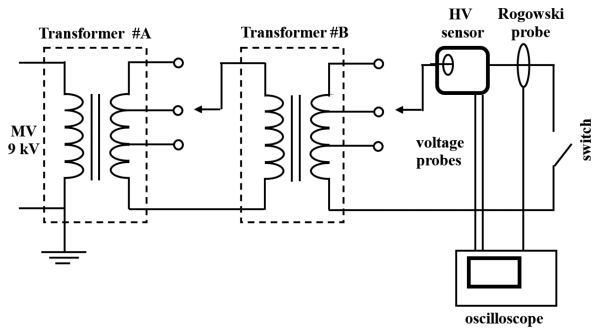

Fig. 11. Schematic of the laboratory setup.

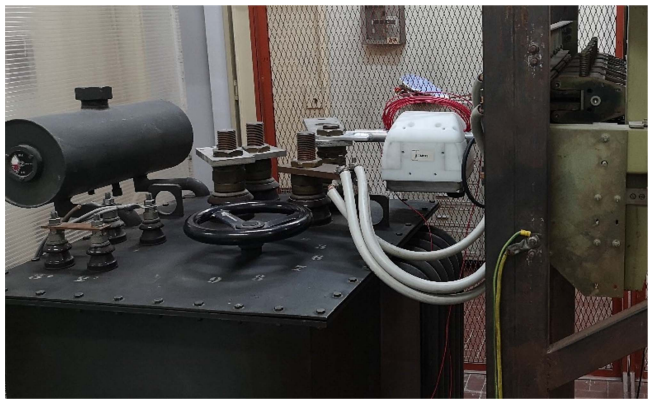

Fig. 12. Picture of the laboratory setup.

when an extremely high line current is present. For the sake of simplicity, the mounting gaps g are in the case neglected, the $B(H)$ characteristic is approximated as a simple saturation, and the order of the successive linear blocks ($T(s)$ and the derivative block s) has been changed. As the amplitude, dI_{ACline} of the input current increases, the block $T(s)$ input will have proportionally increasing amplitude but inversely proportional duration pulses. Considering the band of $T(s)$ much lower than $1/\Delta t$, the output signal of the block $T(s)$ is approximately the pulse response of the block multiplied by the area of the input pulses. In conclusion, as it will be verified in the next section, the resilience to short-circuit phenomena on the AC line is guaranteed by using magnetic materials with a shallow roll-off frequency due to the effect of the laminated structure.

IV. Laboratory Setup

In order to assess the behavior of the EMS in the presence of extreme short-circuit currents on the AC line, an adequate series of numerical and experimental tests were carried out. The practical tests were carried out in the laboratory, where the setup was able to generate typical short circuit currents of High Voltage power systems up to 30 kA. The lab system consists of a power section and a measurement section suitable to carry out the tests with adequate security requirements (for components) and safety (for the operator).

The schematic of the lab system is reported in the following Fig. 11, while Fig. 12 shows a picture taken in the laboratory.

The power supply system is a 9 kV distribution power grid, which feeds a cascade of two power transformers, namely transformer *#A* and transformer *#B*. The transformers operate the reduction of the voltage value to increase the current at the output terminals of transformer *#B*. Both transformers are equipped with tap selectors; moreover, transformer *#B* has a primary winding with four terminals (i.e., the winding consists of two semi-windings).These selectors are used to regulate the transformer chain's voltage ratio properly. The main data of the power transformers are reported in Tables II and III. The sensor under test (i.e., DUT) is installed at one terminal of the transformer *#B* (Fig. 13).

The internal circuitry is activated by an additional winding (depicted in red in Fig. 13) composed of 15 turns which provides

TABLE II
Power Transformer A Main Data

Power [kVA]	500
Input Voltage [V]	9000
Output Voltage [V]	400
Short Circuit Voltage [%]	7

TABLE III
Power Transformer B Main Data

Power [kVA]	50
Input Voltage [V]	230
Output Voltage [V]	40
Short Circuit Voltage [%]	3

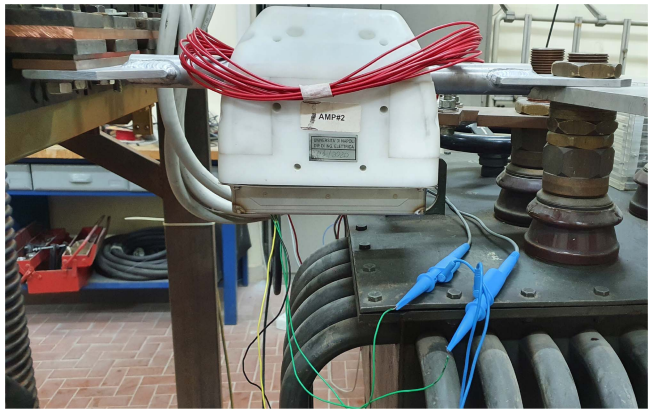

Fig. 13. Detail of the HV sensor.

a 50 Hz sinusoidal current with a rms value equal to 150 Ampereturns.

A controlled switch connects the output terminals of transformer *#B*. When the poles of the switch are disconnected, the circuit is open, and no current flows through the sensor, whereas when the poles of the switch are closed, an electrical current is generated. It is a short-circuit current, being the circuit directly closed on the switch's poles. No additional resistances are present in the circuit. A Rocoil Rogowski probe (30 kA_{rms}, 20 kHz bandwidth) connected to one output terminal of transformer *#B* is used for measuring the short-circuit current; a couple of voltage probes are used to measure the secondary side

voltage V_{tx} (as reported in Fig. 5(a)) in differential mode. In particular, depending on the expected output voltage, alternatively, a couple of Tektronix P5122 probes (100×, 200 MHz bandwidth) or a couple of Agilent N2862B probes (10×, 150 MHz bandwidth) have been adopted. The probes are connected to a four-channel Tektronix DPO3034 oscilloscope.

V. Experimental Results

The sensor under test has been realized with a cylindrical ferromagnetic core whose typical dimensions are $A_e = 1.159$ mm^2 and a $l_e = 0.208$ m. It is made of grain-oriented electrical steel, type M5T30, whose $B(H)$ curve has been modeled using the arctangent function reported in the following relation:

$$B(H) = \frac{\mu_1}{k} atan(Hk) + \mu_2 H \tag{8}$$

where the parameters μ_1, k, and μ_2 have been chosen to have the best fitting of permeability around the origin and residual permeability after saturation [40]. Fig. 14(a) shows the comparison between the $B(H)$ curve reported in the material data sheet and the approximated curve obtained using the model of (8). As can be seen, even if the arctangent function has not a physical meaning, it can satisfactorily reproduce the shape of the B-H curve. The $T(s)$ function is derived by complex permeability, deduced thanks to equivalent impedance measurements carried out adopting a suitable winding on the ferromagnetic core. Fig. 14(b) shows the comparison between the measured complex permeability $\mu' - j\mu''$ (real and imaginary part) derived from the measurements and the real and imaginary part of the transfer function $\mu_r T(s)$ used to approximate it.

At high frequency ($f > 1$ KHz), the trend of the complex permeability can be approximated as $\mu_r \propto \frac{1}{(1+\tau s)^\alpha}$, with α equal to 0.6212 and τ equal to 5.6 ms. This behavior is due to the effect of induced currents and cannot be modeled with the transfer function of a system with a finite number of state variables. In this work, we have chosen to approximate it with a second order transfer function with a zero that at high frequency does not follow the trend exactly, even if it is appropriate for the system description.

In Fig. 15, the power (predicted and measured) extracted at the output of the rectifier of Fig. 7 is reported as a function of V_{bus} for different values of I_{ACline}. As described in Section II and as can be seen from the simulations and measurements, the point of maximum power extraction is dependent on the line's current level I_{ACline}.

Without using an MPPT method and, therefore, keeping the bus voltage fixed under all states, the available power is likely to be significantly lower than the maximum potentially extractable. As an example, in order to highlight the prediction of the model, Fig. 16 shows the main waveforms in the maximum power operating point when I_{ACline} is equal to 80 A rms: in particular, Fig. 16(a) shows the waveshapes $I_{ACline}(t)$, $V_{tx}(t)$

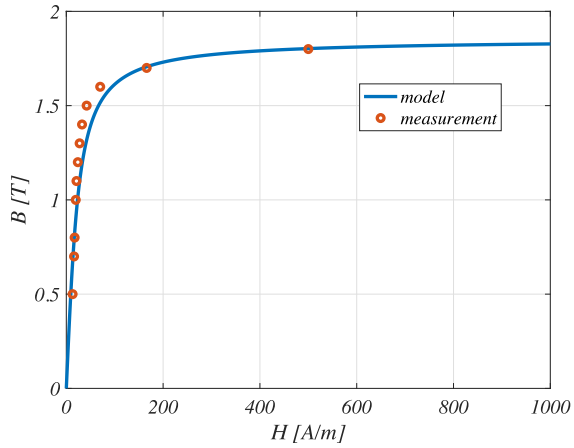

(a)

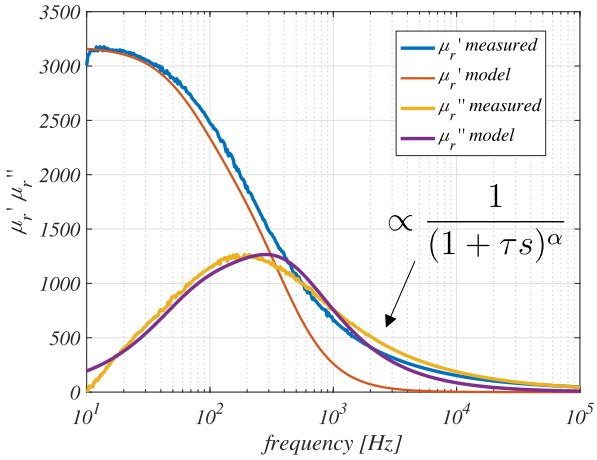

(a)

Fig. 14. (a) Matching between the measured BH curve and that obtained from the model, (b) Matching between the measured permeability values and those obtained from the model $\mu_r T(s)$.

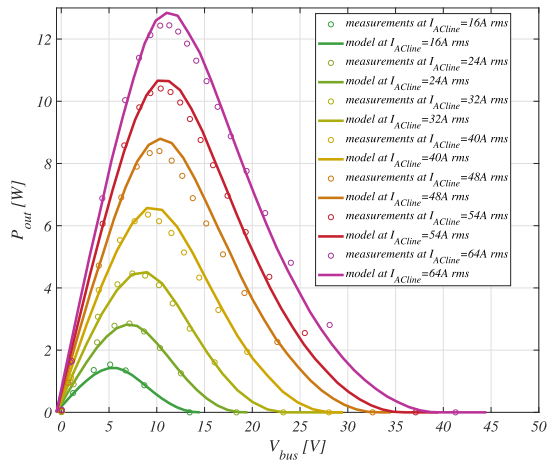

Fig. 15. Matching between the measured $V_{bus} - P_{out}$ curve and that obtained from the model when I_{ACline} has an rms value ranging from 16 A to 64 A.

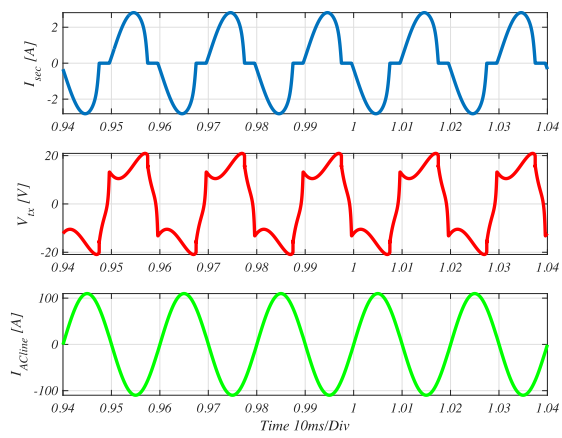

(a)

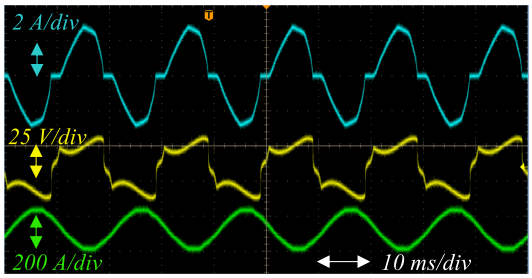

(b)

Fig. 16. Main waveforms in the maximum power point: (a) predicted by the model, (b) measurements.

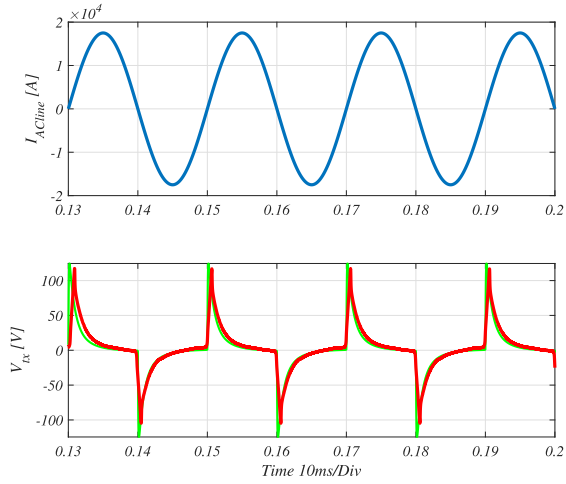

Fig. 17. Main waveforms in short circuit conditions: the short circuit line current I_{ACline} is reported in blue, the measured transformer voltage V_{tx} is reported in red and, in green, the waveform predicted by the model.

and $I_{sec}(t)$ as predicted by the model and Fig. 16(b) shows the same waveforms measured in laboratory.

Finally, the system was tested in high current condition (i.e., 17.5 kA) to verify the effects of a short-circuit on the HV line. The current has been measured by adopting the Rogowski probe with a conversion ratio of 10 kA/V. The main waveforms are reported in Fig. 17. The measured line current I_{ACline} is reported on top of the figure and, at the bottom, the comparison between the measured open circuit transformer voltage V_{tx} (in red) and the waveform predicted by the model (in green) is shown.

VI. Conclusion

Wireless Sensor Networks (WSNs) are systems of distributed sensor nodes allowing the real-time monitoring of power lines in terms of physical, mechanical, and environmental operating conditions. The planning of the sensor nodes in terms of power requirements and energy management systems is related to the study of technical solutions operating in the presence of relevant electromagnetic field environments. The paper investigated the design of a sensor Energy Management System (EMS) for HV power line application. The EMS is energized by the electromagnetic field harvester method. The proposed solution used a supercapacitor as a storage device and a Maximum Power Point Tracker (MPPT) system, which charges the storage unit by magnetic coupling with the actual electrical current flowing in the power line. The MPPT system's functionality was based on the non-linear characteristic and frequency behavior of the magnetic permeability of the ferromagnetic core. The detailed analytical model of the physics of the system was discussed. A low pass filter $T(s)$ was introduced in the model in order to account for the frequency behavior of the permeability. The two critical impedance parameters placed in parallel with the current source and the maximum voltage were investigated in ordinary and extraordinary conditions. In particular, in the presence of high short-circuit conditions, it was pointed out the relevant function of the frequency behavior of the laminated material. The results of experimental lab measurements carried out on a realized prototype verified the goodness of the design modeling and the resilience of the device, guaranteed by using magnetic materials with a low roll-off frequency.

References

[1] F. M. de Vasconcelos, C. Santos Rocha, C. F. Meschini Almeida, D. de Souza Pereira, L. H. Leite Rosa, and N. Kagan, "Methodology for inspection scheduling in power distribution networks based on power quality indexes," *IEEE Trans. Power Del.*, vol. 36, no. 2, pp. 1211–1221, Apr. 2020.

[2] S. Verma, S. Jaiswal, A. Rawat, and A. K. Singh, "IoT based three phase transmission line fault detection," in *Proc. Int. Conf. Comput. Commun. Informat.*, 2022, pp. 1–4.

[3] E. Fontana, S. Oliveira, F. Cavalcanti, R. Lima, J. Martins-Filho, and E. Meneses-Pacheco, "Novel sensor system for leakage current detection on insulator strings of overhead transmission lines," *IEEE Trans. Power Del.*, vol. 21, no. 4, pp. 2064–2070, Oct. 2006.

[4] J. Z. C. Jiang, J. Xie, and X. Zhang, "A novel high-voltage transmission line joint temperature monitoring system using hybrid communication networks," *IEEE Access*, vol. 9, pp. 109478–109487, 2021.

[5] L. Silvestri et al., "A novel optical sensing technology for monitoring voltage and current of overhead power lines," *IEEE Sensors J.*, vol. 21, no. 23, pp. 26699–26707, Dec. 2021.

[6] T. Zhuang, M. Ren, X. Gao, M. Dong, W. Huang, and C. Zhang, "Insulation condition monitoring in distribution power grid via IoT-based sensing network," *IEEE Trans. Power Del.*, vol. 34, no. 4, pp. 1706–1714, Aug. 2019.

[7] M. A. Matin and M. N. Islam, "Overview of wireless sensor network," in *Wireless Sensor Networks - Technology and Protocol*, London, UK: InTech, Sep. 2012, doi: 10.5772/49376.

[8] Y. Shi, X. Cui, L. Qi, X. Zhang, X. Li, and H. Shen, "A novel energy harvesting method for online monitoring sensors in HVDC overhead line," *IEEE Trans. Ind. Electron.*, vol. 70, no. 2, pp. 2139–2143, Feb. 2023.

[9] F. Guo, H. Hayat, and J. Wang, "Energy harvesting devices for high voltage transmission line monitoring," in *Proc. IEEE Power Energy Soc. Gen. Meeting*, 2011, pp. 1–8.
[10] V. C. Gungor and G. P. Hancke, "Industrial wireless sensor networks: Challenges, design principles, and technical approaches," *IEEE Trans. Ind. Electron.*, vol. 56, no. 10, pp. 4258–4265, Oct. 2009.
[11] S. Yeesparan, M. Z. Bin Baharuddin, and N. B. M. Din, "A review of energy harvesting methods for power transmission line monitoring sensors," *Int. J. Eng. Technol.*, vol. 7, no. 4.35, pp. 153–161, 2018.
[12] C. Bernauer, H. Böhme, and S. Grossmann, "Temperature measurement on overhead transmission lines (OHTL) utilizing surface acoustic wave (SAW) sensors," in *Proc. 19th Int. Conf. Electricity Distrib.*, 2007, Art. no. 0788.
[13] H. Zangl, T. Bretterklieber, and G. Brasseur, "A feasibility study on autonomous online condition monitoring of high-voltage overhead power lines," *IEEE Trans. Instrum. Meas.*, vol. 58, no. 5, pp. 1789–1796, May 2009.
[14] J. Ramirez-Nino, M. J. O. Pacheco, J. Rodriguez, and V. M. Castano, "Design and construction of a pollution monitor for power line insulators," *Meas. Sci. Technol.*, vol. 7, pp. 876–881, 1996.
[15] H. Boxuan, S. Xiao-Lei, Z. Jin, and C. Zhi-Gang, "Thermoelectrics for medical applications: Progress, challenges, and perspectives," *Chem. Eng. J.*, vol. 437, 2022, Art. no. 135268.
[16] W. Chongfeng and J. Xingjian, "A comprehensive review on vibration energy harvesting: Modelling and realization," *Renew. Sustain. Energy Rev.*, vol. 74, pp. 1–18, 2017.
[17] M. Zhu, P. Baker, N. Roscoe, M. Judd, and J. Fitch, "Alternative power sources for autonomous sensors in high voltage plant," in *Proc. IEEE Elect. Insul. Conf.*, 2009, pp. 36–40.
[18] B. Garcia, J. Burgos, and A. Alonso, "Transformer tank vibration modeling as a method of detecting winding deformations - Part II: Experimental verification," *IEEE Trans. Power Del.*, vol. 21, no. 1, pp. 164–169, Jan. 2006.
[19] I. Paprotny, Q. Xu, W. W. Chan, R. M. White, and P. K. Wright, "Electromechanical energy scavenging from current-carrying conductors," *IEEE Sensors J.*, vol. 13, no. 1, pp. 190–201, Jan. 2013.
[20] F. Yang, L. Du, H. Yu, and P. Huang, "Magnetic and electric energy harvesting technologies in power grids: A review," *Sensors*, vol. 20, 2020, Art. no. 1496.
[21] X. Zeng, Z. Yang, P. Wu, L. Cao, and Y. Luo, "Power source based on electric field energy harvesting for monitoring devices of high voltage transmission line," *IEEE Trans. Ind. Electron.*, vol. 68, no. 8, pp. 7083–7092, Aug. 2021.
[22] O. Menendez, F. A. Auat Cheein, and J. Rodriguez, "Displacement current-based energy harvesters in power grids: Topologies and performance evaluation," *IEEE Ind. Electron. Mag.*, vol. 16, no. 3, pp. 52–66, Sep. 2022.
[23] W. Wang, X. Huang, J. Tan Guo, and H. Liu, "Optimization design of an inductive energy harvesting device for wireless power supply system overhead highvoltage power lines," *Energies*, vol. 9, 2016, Art. no. 242.
[24] J. D. Boles, B. Ozpineci, L. M. Tolbert, T. A. Burress, C. W. Ayers, and J. A. Baxter, "Inductive power harvesting for a touchless transmission line inspection system," in *Proc. IEEE Power Energy Soc. Gen. Meeting*, 2016, pp. 1–5.
[25] Z. Qian, J. Wu, X. He, and Z. Lin, "Power maximised and antisaturation power conditioning circuit for current transformer harvester on overhead lines," *IET Power Electron.*, vol. 11, no. 14, pp. 2271–2278, 2018.
[26] J. Wang and S. Ha, "A wide input power line energy harvesting circuit for wireless sensor nodes," in *Proc. IEEE Int. Symp. Circuits Syst.*, 2021, pp. 1–5.
[27] J. Wang and W. Chen, "Output characteristics analysis of energy harvesting current transformer," *IEEE Sensors J.*, vol. 21, no. 20, pp. 22595–22602, Oct. 2021.
[28] S. Yuan, Y. Huang, J. Zhou, Q. Xu, C. Song, and G. Yuan, "A high-efficiency helical core for magnetic field energy harvesting," *IEEE Trans. Power Electron.*, vol. 32, no. 7, pp. 5365–5376, Jul. 2017.
[29] R. M. White, D. Nguyen, Z. Wu, and P. K. Wright, "Atmospheric sensors and energy harvesters on overhead power lines," *Sensors*, vol. 18, 2018, Art. no. 114.
[30] S. Sinha, S. Maji, and K. Afridi, "Comparison of large air-gap inductive and capacitive wireless power transfer systems," in *Proc. IEEE Appl. Power Electron. Conf. Expo.*, 2021, pp. 1604–1609.
[31] T. Taithongchai and E. Leelarasmee, "Adaptive electromagnetic energy harvesting circuit for wireless sensor application," in *Proc. 6th Int. Conf. Elect. Eng./Electron. Comput. Telecommun. Inf. Technol.*, 2009, pp. 278–281.
[32] J. Wang, J. Kim, and D. S. Ha, "Powerline energy harvesting circuit with a desaturation controller for a magnetic core," in *Proc. IEEE Int. Midwest Symp. Circuits Syst.*, 2021, pp. 220–223.
[33] J. Moon and S. B. Leeb, "Power electronic circuits for magnetic energy harvesters," *IEEE Trans. Power Electron.*, vol. 31, no. 1, pp. 270–279, Jan. 2016.
[34] M. Sarker, M. Saad, J. Olazagoitia, and J. Vinolas, "Review of power converter impact of electromagnetic energy harvesting circuits and devices for autonomous sensor applications," *Electronics*, vol. 10, 2021, Art. no. 1108.
[35] B. Conway, *Electrochemical Supercapacitors: Scientific Fundamentals and Technological Application*. Norwell, MA, USA: Kluwer, 1999.
[36] D. Newell and M. Duffy, "Review of power conversion and energy management for low-power, low-voltage energy harvesting powered wireless sensors," *IEEE Trans. Power Electron.*, vol. 34, no. 10, pp. 9794–9805, Oct. 2019.
[37] A. S. Weddell, G. V. Merrett, T. J. Kazmierski, and B. M. Al-Hashimi, "Accurate supercapacitor modeling for energy harvesting wireless sensor nodes," *IEEE Trans. Circuits Syst. II: Exp. Briefs*, vol. 58, no. 12, pp. 911–915, Dec. 2011.
[38] Y. Zhang and H. Yang, "Modeling and characterization of supercapacitors for wireless sensor network applications," *J. Power Sources*, vol. 196, no. 8, pp. 4128–4135, 2011.
[39] Z. Wang et al., "An enhanced energy harvesting method based on resonant current transformer for high voltage ac cable monitoring equipment," in *Proc. IEEE Appl. Power Electron. Conf. Expo.*, 2014, pp. 3455–3459.
[40] M. M. Ponjavic and M. R. Duric, "Nonlinear modeling of the self-oscillating fluxgate current sensor," *IEEE Sensors J.*, vol. 7, no. 11, pp. 1546–1553, Nov. 2007.

Massimo Ferracini born in 1970. He received the bachelor's degree from the University of Udine, Udine, Italy, in 1996. Since 2012, has been an hardware and software Engineer. He is currently with Telecommunication Company, Calzavara S.p.A., Udine, Italy, as high power LED control and driver board designer for obstruction lights systems (AWCL) and heliports landing path. The company develops and sells its light systems worldwide. Hid previous work experiences include ten years video board designer for HD and 4k video projection system and control board designer for air conditioning and heater systems.

Mario Pagano (Senior Member, IEEE) was born in Naples, Italy, in 1970. He received the M.Sc. (Hons.) and the Ph.D. degrees in electrical engineering from the University of Naples Federico II, Naples, Italy, in 1995 and 1999, respectively. In 2002, he was appointed as a Researcher of power systems with the University of Naples Federico II. He is currently an Associate Professor. He is author or co-author of more than 120 scientific papers published in reviewed journals and presented at international and national conferences. His research interests include transmission power systems, renewable sources, storage systems, and electrical systems for mobility.

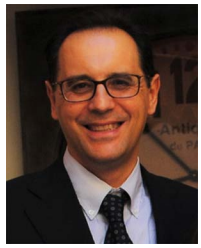

Carlo Petrarca (Member, IEEE) received the Doctor degree in electric engineering in 1993, and the Ph.D. degree in electrical engineering from the University of Naples Federico II, Naples, Italy, in 1997. He is currently an Associate Professor of electrical engineering with the Department of Electrical Engineering and Information Technology, University of Naples Federico II, teaching courses on basic circuit theory, high voltage techniques and diagnostics, and characterization and modelling of materials for electrical engineering. His research interests include high voltage testing and modeling, non-destructive testing of components, electromagnetic characterization and treatment of innovative materials, and complex networks analysis.

Eric Polo received the M.S. degree in electronic engineering from the University of Padua, Padua, Italy. From 2000 to 2004, he was with Seima Elettronica as a junior Electronic Engineer. From 2005 to 2012, he was with SIM2 Multimedia in Pordenone, Italy, where he followed, as a Project Manager, the develop of the Video projectors for Home Cinema. In 2013, he joined Calzavara S.p.A., Basiliano (UD), Italy, as the Chief of R&D, working on lamp for AWL (Aviation Warning Lights).

Stefano Saggini (Member, IEEE) received the M.S. degree in electronic engineering and the Ph.D. degree in information engineering from the Politecnico di Milano, Milano, Italy, in 2000 and 2004, respectively. In 2004, he joined STMicroelectronics, Industrial and Power Supply Division. Since December 2006, he has been with the Polytechnic Department of Engineering and Architecture, University of Udine, Udine, Italy. His research interests include modeling and digital control techniques for power systems. Dr. Saggini was the recipient of the Prize Paper Award for the IEEE Transactions on Power Electronics in 2004 and in 2019.

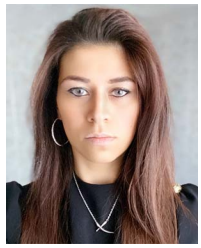

Giulia Segatti (Graduate Student Member, IEEE) received the B.S. degree in electronics engineering and the M.S. degree in robotics and industrial automation in 2019 and 2021, respectively, from the University of Udine, Udine, Italy, where she is currently working toward the Ph.D. degree in industrial and information engineering. Her research interests focuses on magnetic design in power converters and wireless charging.

Mario Ursino (Member, IEEE) received the B.S. degree in electronics engineering and the M.S. degree in robotics and industrial automation from the University of Udine, Udine, Italy, in 2013 and 2016, respectively. He received the Ph.D. degree in industrial and information engineering from the University of Udine, working with STmicroelectronics of Agrate, Italy, in 2019. He had several collaborations with STmicroelectronics, Infineon Technologies, Google Inc. and CERN. During the Ph.D. degree, he published several articles in international conferences and journals. He is currently a System Innovation Engineer in Infineon Technologies Austria, developing very high-density DC–DC topologies for AI data-center applications, ranging from intermediate bus converters to point-of-load converters. His research interests include planar electromagnetic research, power system automatic control, power integrity analysis, and wireless power transfer.